J. Chem. Sci. (2021)133:26
https://doi.org/10.1007/s12039-021-01889-3

REGULAR ARTICLE

Ordered structure induced in human c-Myc PEST region upon forming a disulphide bonded dimer

MOHD ZIAUDDIN ANSARI, SHAH EKRAMUL ALOM and RAJARAM SWAMINATHAN*
Department of Biosciences and Bioengineering, Indian Institute of Technology Guwahati, Guwahati, Assam 781 039, India
E-mail: rsw@iitg.ac.in

MS received 15 August 2020; revised 16 December 2020; accepted 30 December 2020

Abstract. PEST rich protein sequences are intrinsically disordered and serve as degradation hotspots in eukaryotic cells. The structure of PEST degrons in proteins and their mechanism of action remain poorly understood. Deregulation or overexpression of human transcription factor c-Myc causes cancer. The PEST region in c-Myc is implicated for its rapid degradation. Here, we investigate how the structure of 77-residue PEST fragment of c-Myc and its mutant (M1, Trp inserted) are affected by the formation of a covalent dimer. DLS and size exclusion data indicated a ∼ 30% increase in Stokes radius upon the formation of the dimer. CD showed an increase in helix and strand content with dimer formation in both Wt and mutant. However, counterintuitively, Trp fluorescence anisotropy decay was marginally faster in the dimer compared to monomer. This anomaly was traced to Trp-Trp Förster resonance energy homotransfer in M1 dimer, suggesting close interaction between two chains in the dimer. Our data suggest that indole rings in the PEST M1 dimer are no further than 24 Å apart. These results may hold the key to higher stability of c-Myc in tumours and the poorly understood physiological role of c-Myc oligomer in cells.

Keywords. Cys-linked dimer; Protein half-life; Trp-Trp homoFRET; IDR dimer; Cancer.

Abbreviations

DTNP	2,2′-Dithiobis(5-nitropyridine)
FWHM	Full Width at Half Maximum
Gdn.HCl	Guanidine hydrochloride
IDP	Intrinsically disordered protein
IRF	Instrument Response Function
MEM	Maximum entropy method
NATA	N-Acetyl-L- Tryptophan Amide
PEST Wt	PEST Wild type
PEST M1	PEST Mutant1
TCEP	Tris (2-carboxyethyl) Phosphine

1. Introduction

Intrinsically disordered proteins function as regulators in several critical cellular activities.[1,2] The structure and molecular motions of IDPs are important to understand their functional mechanisms.[2,3] IDP dimers although prevalent in nature, are not well-studied. Some IDPs like Sml1[4] display function as a dimer. Considering that IDPs are themselves robust dynamic conformational ensembles, it is worthwhile to determine if dimer formation can influence IDP structure and molecular motions. Using c-Myc (human) PEST fragment, this forms the main objective of this paper.

In humans, the c-Myc oncoprotein (Figure 1a) is involved in vital processes such as cell growth, proliferation, differentiation and apoptosis.[5,6] The expression of c-Myc is tightly controlled during initiation of transcription, translation and protein stability.[6,7] A wide range of cancers like lymphoma, leukaemia and ovarian, lung, colon and breast cancer[7] are caused by deregulation or overexpression of c-Myc, a transcription factor. This transcription factor is also unstable and normally degrades within 30 min like other transcription factors c-Jun[8] and c-Myb[9] which are short-lived. c-Myc sequence contains i) an unstructured transcriptional activation domain[10] at N-terminus, ii) a helix-loop-helix region[11,12] at C-terminus and iii) a disordered central PEST region

*For correspondence

Supplementary Information: The online version of this article (https://doi.org/10.1007/s12039-021-01889-3) contains supplementary material, which is available to authorized users.

Published online: 26 February 2021

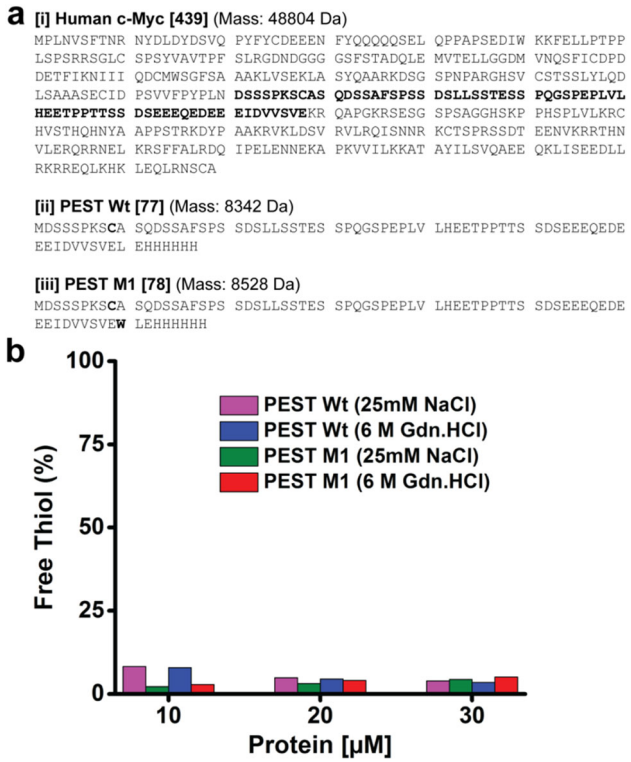

Figure 1. (**a**) Primary structure of (i) c-Myc (human); amino acids represented in bold denote the PEST region; (ii) PEST Wt and (iii) PEST M1 are shown (where Cys/Trp are represented in bold). (**b**) Percentage of free thiol group present in 10-30 μM PEST Wt and PEST M1 in Tris [25 mM]; pH 7.4 and Gdn.HCl [6 M], respectively using 50 μM of DTNP at room temperature (298 K) is shown.

(amino acids 201 to 268), with an abundance of **P** (Pro), **E** (Glu), **S** (Ser) and **T** (Thr).[13] Contrary to N and C terminal domains whose function and structure are well recognized,[14] functions of c-Myc PEST region is poorly understood and its 3D structure remains unknown.

PEST regions were first discovered among short-lived intracellular proteins of eukaryotic origin. PEST region accounted for their rapid degradation.[13,15] Like c-Myc; p53, Jun, Fos, and ODC also have PEST region and degrade rapidly.[13] The C-terminal region of monomeric PEST fragment from human c-Myc was shown to acquire structure at acidic pH.[16] In this work, we investigate how the structure of the same fragment is altered upon forming a disulphide linked dimer.

2. Experimental

Chemicals/Reagents: TCEP (C4706); Guanidine Hydrochloride (G3272); DTNP (158194); L-Cysteine (168149); and NATA (A6501) were procured from Sigma Aldrich, Bangalore, India. Moreover, all salts and buffers were obtained from Merck India Limited. All chemicals used were of analytical grade (≥98% purity).

Figure 1a displays the primary structure of PEST Wt (c-Myc (human); region 201-268; P01106 Uniprot) and PEST M1 (Trp inserted mutant). The purpose of creating PEST M1 was to probe protein structural dynamics in the vicinity of C-terminus by measuring Trp fluorescence.

2.1 *Expression of PEST fragments and their purification*

The PEST fragments (PEST Wt and M1) of human c-Myc were expressed in *E.coli* and purified as reported earlier.[17]

2.2 *Estimation of free thiol*

To determine the concentration of free thiol in the PEST peptide, DTNP assay was performed as reported earlier.[18] 50 μM of DTNP was mixed with the 10, 20 and 30 μM of PEST fragments dissolved in the reaction buffer (Tris [25 mM] + NaCl [25 mM]; pH 7.4). For calculating free thiol concentration in PEST fragments in denatured condition, 10, 20, 30 μM PEST Wt and M1 was mixed with buffer (Tris [25 mM] + NaCl [25 mM] + Gdn.HCl [6 M]; pH 7.4) and subjected to overnight incubation at room temperature (298 K). Overnight incubated PEST samples in Gdn.HCl [6 M] were used to determine free thiol. Figure S1a and b display the standard plots for a known concentration of L-cysteine in standard (Tris [25 mM]) and denatured (Gdn.HCl [6 M]) conditions, respectively.

2.3 *Mass analysis*

Mass determination of PEST fragments were carried out by Daltonics Bruker MALDI-TOF mass spectrometer as reported earlier.[17] Mass of PEST monomer was determined under reducing environment by dissolving the protein in water which contains 6 mM β Mercaptoethanol, while a mass of PEST dimer was determined under non-reducing condition by solubilizing protein in deionized water.

2.4 *Size Exclusion Chromatography*

To separate the PEST Wt/M1 dimer from their monomer, SEC was performed (ÄKTApurifier^{TM}

FPLC; GE Healthcare) as reported earlier.[16] 300 μM (1 mL) of PEST Wt/M1 was loaded on the column and subsequently, the elution was performed using elution buffer (Tris [25 mM] + NaCl [25 mM]; pH 7.4). All standards (Figure S2a) and samples were allowed to run with a flow rate of 1 mL/minute throughout the experiment. The molecular weight of PEST fragments was calculated using a standard curve (Figure S2b, Supplementary Information).

2.5 *Dynamic Light Scattering (DLS) analysis*

DLS experiments were carried out by Zetasizer Nano ZS 90 as described earlier.[16] To determine the hydrodynamic radius, 1.5 mg per mL of monomeric and dimeric PEST Wt/M1 (separated from SEC) were mixed in the reducing (Tris [25 mM] + TCEP [1 mM] + NaCl [25 mM]; pH 7.4) and non-reducing (Tris [25 mM] + NaCl [25 mM]; pH 7.4) buffers, respectively. TCEP was added for preventing dimerization in PEST fragment by blocking its disulphide linkage formation.

2.6 *Circular Dichroism*

CD spectra of monomeric and dimeric PEST Wt /M1 were collected on a Jasco J-1500 CD spectrometer as described previously.[17] To collect the CD spectra, monomeric and dimeric PEST Wt/M1 [20 μM] was added in reducing (Tris [5 mM] + TCEP [1 mM]; pH 7.4) and non-reducing (Tris [5 mM]; pH 7.4) buffers, respectively. Secondary structure contents were calculated using CDSSTR program and reconstructed spectra were well superimposed on experimental spectra (Figure S4, Supplementary Information).

2.7 *Steady-state fluorescence analysis*

Fluorescence emission and anisotropy (Steady state) of PEST M1 Trp, were collected using Fluoromax-4 Spectrofluorometer as reported earlier.[16] Excitations were done at 295 nm (1 nm slit), and emission 310-500 nm and at 345 nm (for anisotropy, 5 nm slit) was collected at 298 K. For fluorescence intensity and anisotropy measurements of Trp, 20 μM of monomeric and 10 μM of dimeric PEST M1 was dissolved in reducing (Tris [25 mM] + TCEP [5 mM] + NaCl [25 mM]; pH 7.4) and non-reducing (Tris [25 mM] + NaCl [25 mM]; pH 7.4) buffers, respectively.

2.8 *Trp-Trp energy transfer measurements*

For Trp-Trp energy transfer measurements, the polarization of Trp emission was measured. For this, solutions of 15 μM Human Serum Albumin; 25 μM PEST M1 dimer (dissolved in non-reducing buffer) or 50 μM PEST M1 monomer (dissolved in reducing buffer) were excited at 295nm (1 nm slit) and 310 nm (5 nm slit) and their emission were recorded at 345 nm (15 nm slit) at 298 K.

2.9 *Time-resolved fluorescence*

Trp fluorescence lifetime of PEST M1 and anisotropy decay measurements were carried out by time-correlated single-photon counting method (Delta-Pro^{TM} NanoLEDs, Horiba UK), as reported earlier.[16] Excitation was done using, 295 nm pulsed LED; vertically polarized light with 20 MHz repetition rate; ~ 810 ps (FWHM) IRF. Total Trp emission (20,000 peak counts; 2202 channels; 28 ps/channel) was collected by blocking the excitation light with 320 nm long pass filter. At least three independent decay measurements were recorded at 25 °C for each sample condition. Lifetime (τ_i) and amplitudes (α_i) were extracted from fluorescence intensity decay as described previously.[16,19,20] Fluorescence lifetime distributions from Trp fluorescence intensity decay was obtained using MEM as reported previously.[16,21,22]

Rotational correlation times of PEST M1 Trp was extracted from polarized intensity decays ($I_{\|}$) and ($I_{\perp}$) as reported earlier.[16,18,20,23] In each case, evaluation for best fit was done by visual inspection of randomness in residuals, comparison with steady-state anisotropy value and reduced χ^2.

3. Results and Discussion

3.1 *Estimation of a free thiol group*

To investigate the dimer formation in PEST fragment and nature of interactions involved in its dimerization, estimation of free thiol group was performed. Figure 1b shows a significantly lower amount of free thiol present in PEST Wt and M1 in Tris [25 mM]; pH 7.4. This may be due to involvement of free cysteine in the dimer formation of PEST fragment through disulphide bond or free cysteine may not be available to react with DTNP because of its buried nature either inside the protein core or within the formed dimer. To resolve this, DTNP assay was performed in Gdn.HCl [6 M] for unfolding and expose the free cysteine in

PEST. However, even in Gdn.HCl [6 M], insignificant increase in free thiol of PEST Wt and M1 was observed (Figure 1b). Further, attempts to label PEST fragment in non-reducing condition using iodoacetamide derivative of dansyl probe which reacts with the free thiol group of cysteine were unsuccessful. However, labelling of dansyl group to PEST fragment was successful in a reducing environment.[16] The availability of fewer free thiol in Gdn.HCl [6 M] and the necessity for a reducing condition for iodoacetamide reaction clearly hint at involvement of free thiol in the dimer formation through disulphide bond.

3.2 *Reducing, non-reducing SDS-PAGE and mass analysis of PEST dimer*

To confirm the involvement of free cysteine in dimerization of PEST fragment through disulphide bond formation, 15% non-reducing and reducing SDS-PAGE analysis was carried out. Non-reducing SDS-PAGE (Figure 2c-d) shows a mixture of both monomeric and dimeric bands. While reducing SDS-PAGE (Figure 2a-b), displays only monomeric band of PEST fragments as β-Mercaptoethanol caused reduction of the disulphide bond. This result clearly shows dimerization of PEST fragment occurs by disulphide bond formation.

Both monomeric and dimeric PEST Wt and PEST M1 show anomalous behaviour on the non-reducing SDS-PAGE with apparent Molecular Weight (MW) of 15 kDa and 28 kDa, respectively. This anomalous nature of PEST monomer and dimer on SDS-PAGE hints toward the presence of disordered structure and has been reported in many IDPs.[24]

To determine the exact MW of PEST dimer, mass spectra of PEST Wt and M1 were collected. These show the presence of monomeric and dimeric forms of PEST fragments under the non-reducing conditions (Figure 2e). However, in reducing environment only the monomeric forms of PEST fragment are seen.[17] The actual molecular mass of PEST Wt and M1 dimer, determined by mass spectrometry was 16,681 and 17,050 Da, respectively. However, PEST dimer shows about a 1.7-fold increase in its MW (about 28 kDa), determined by non-reducing SDS-PAGE owing to its unusual amino acid composition that binds to less SDS compared to normal protein.[24]

Hence, mass spectrometry investigations establish the dimer formation in PEST fragment by disulphide bond formation. This dimerization of PEST fragment and its disordered behaviour encouraged us further to extract its structural information.

3.3 *Size exclusion chromatography and dynamic light scattering studies of PEST Dimer*

To probe the structural properties of PEST dimer, it was separated from PEST monomer using SEC. Figure 3a displays the chromatographic elution pattern for PEST Wt and PEST M1 under non-reducing

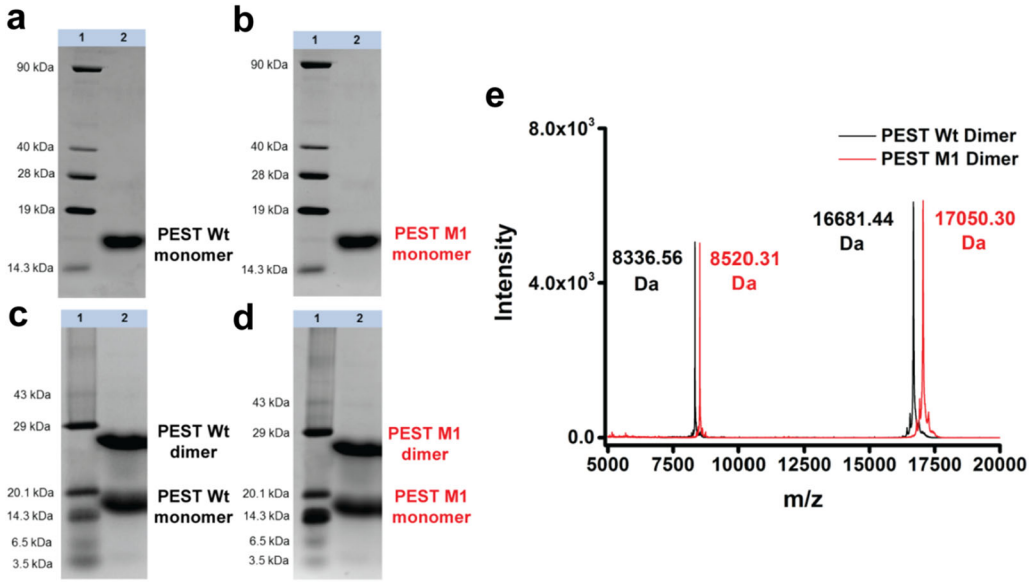

Figure 2. 15% reducing SDS-PAGE of, (**a**) PEST Wt; (**b**) PEST M1 and non-reducing SDS-PAGE of, (**c**) PEST Wt; (**d**) PEST M1 showing monomeric and dimeric bands of purified protein (**e**) Mass spectra of dimeric PEST fragments under non-reducing condition, showing mixture of monomeric and dimeric population in both PEST Wt and M1. The mass of dimeric PEST Wt and M1 calculated from sequence were 16,681.22 and 17,053.64 Da.

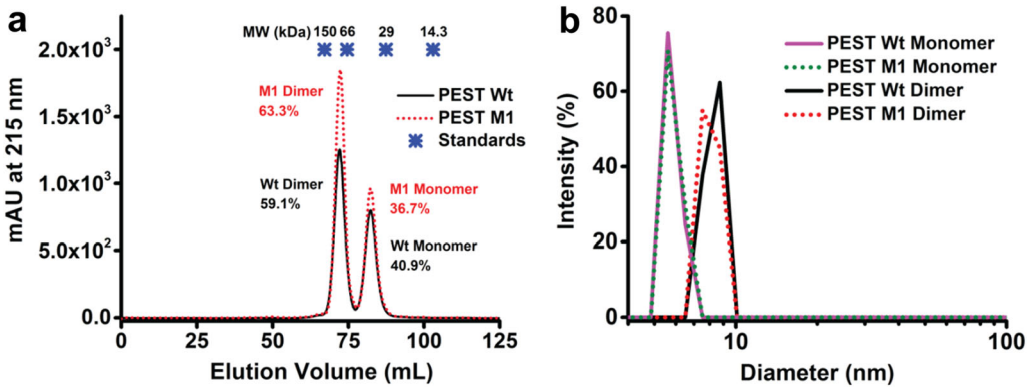

Figure 3. (**a**) Elution profile of gel permeation chromatography for PEST Wt and M1; at 215 nm, showing the mixture of monomer and dimer. Both PEST Wt and M1 were eluted with non-reducing elution buffer (Tris [25 mM] + NaCl [25 mM]; pH 7.4) at room temperature. Asterisks represent the position of the elution for standards. (**b**) Hydrodynamic diameter of PEST Wt; M1 monomer and dimer [1.5 mg/mL] dissolved in reducing (Tris [25 mM]+ TCEP [1 mM] + NaCl [25 mM]; pH 7.4) and non-reducing buffer (Tris [25 mM]+ NaCl [25 mM]; pH 7.4), respectively at 298 K is shown.

condition. Both PEST Wt and M1 displayed separate elution peaks for monomeric and dimeric population. Monomeric PEST Wt and M1 eluted with 82.31 and 82.43 mL whereas, their dimers displayed 72.19 and 72.37 mL of elution volume, respectively. The population of monomeric PEST Wt and M1 estimated from their area under elution peak was 40.9% and 36.7%; whereas their dimeric population was 59.1% and 63.3%, respectively. Apparent MW of monomeric and dimeric PEST fragments are displayed in Table 1. This apparent MW of PEST monomer and dimer was around 5.5 times greater than its real mass (determined by mass spectrometry) and reveals the presence of random coil structure as previously established in several IDPs.[25] Further, the monomer and dimer forms of PEST Wt and M1 both fall in the fitted line (Figure S2b, Supplementary Information) suggesting their similar shapes.

Additionally, to get more insight about hydrodynamic properties of PEST Wt and M1, their Stokes radii (R_s) were calculated from SEC data (Table 1 and Figure S2c, Supplementary Information). The larger Stokes radii value among PEST Wt and M1 dimer in comparison to their respective monomers, clearly reveals expanded volume in the dimer compared to the monomer.

To directly determine and validate the Stokes radius of PEST estimated by SEC, DLS measurements were performed (Figure 3b and Table 1). These Stokes radii values of PEST fragments closely match with the values estimated by SEC. Correlogram of PEST dimer shows the longer decay time than PEST monomer (Figure S3, Supplementary Information). This is attributed to a larger hydrodynamic size of dimer as compared to monomeric PEST fragment. To obtain information on the secondary structure, we performed the Circular Dichroism experiments on monomeric and dimeric PEST fragment.

Table 1. Stokes radius, apparent molecular weight and percentage of unordered structure in monomeric and dimeric PEST fragment at pH 7.4. Values in brackets indicate standard deviations for n = 3.

	PEST Monomer		PEST Dimer	
Protein property	Wt	M1	Wt	M1
Stokes radius (SEC) (in nm)	3.11 (0.03)	3.10 (0.05)	3.95 (0.01)	3.93 (0.02)
Stokes radius (DLS) (in nm)	3.14 (0.21)	3.13 (0.19)	4.19 (0.20)	4.12 (0.08)
Apparent Mol. Wt. (SEC) (in kDa)	46.54 (1.22)	45.98 (2.05)	91.85 (0.04)	90.71 (0.12)
Unordered Structure (CD) (in %)	54	57	34	45

3.4 *Circular Dichroism Analysis of PEST Wt and M1 dimer*

Figure 4a depicts the comparison of CD spectra of dimeric PEST fragments with their monomers. CD spectra of both PEST Wt and M1 monomer are nearly superimposable, revealing peak of negative ellipticity at 201 nm whereas, their dimer display negative ellipticity peak at 205 and 202 nm, respectively. PEST Wt dimer shows more negative ellipticity at 205 and 222 nm in comparison with PEST M1 dimer. This higher negative ellipticity of PEST Wt dimer at 222 nm suggests a gain of more ordered structure than PEST M1 dimer. PEST Wt dimer displays more α-helix content than PEST M1 dimer. However, PEST Wt and M1 dimer consistently reveal a decrease in their disorder content in comparison with PEST Wt and M1 monomer (Figure 4b and Table 1 *last row*). Secondary structure analysis clearly indicates a significant structural gain in PEST dimers as compared to their monomers. However, PEST Wt and PEST M1 retain significant structural disorder after dimerization.

To observe the local structure and nanosecond rotational dynamics of PEST M1 dimer along with its monomer at C-terminus, we monitored the intrinsic luminescence of Trp^{70} that was specifically placed for this purpose.

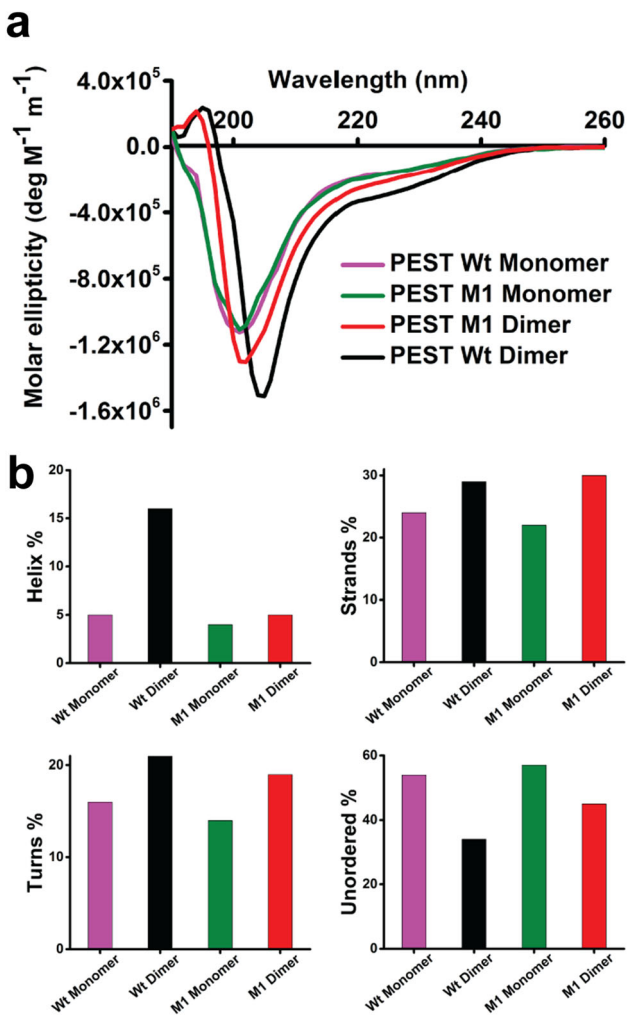

Figure 4. (**a**) CD spectra of monomeric and dimeric PEST Wt and PEST M1 [20 μM], recorded at room temperature. Monomeric PEST fragment was mixed in reducing (Tris [5 mM] + TCEP [1 mM]; pH 7.4) and dimeric PEST fragment was dissolved in non-reducing (Tris [5 mM]; pH 7.4) buffers, respectively. (**b**) Secondary structure information in monomeric and dimeric PEST Wt and PEST M1, calculated by CDSSTR program.

3.5 *Trp fluorescence of PEST M1 Dimer*

Trp fluorescence emission (steady state) of PEST M1 was monitored to explore the local environment around the inserted Trp. PEST M1 dimer and monomer display Trp emission peak at 346 nm while, NATA (Trp derivative) displays maximum at 349 nm, which is expected since the indole ring is completely exposed to water (Figure 5a). The emission peaks of monomeric and dimeric PEST M1 Trp at 346 nm, hints its significant exposure to water and interestingly no change in solvent exposure upon forming the dimer. Additionally, to gain more insights about the structural dynamics of PEST M1, steady state fluorescence anisotropy (r_{ss}) analysis of its Trp was performed. The Trp fluorescence anisotropy value of PEST M1 in monomer, dimer and NATA was 0.051 ± 0.005, 0.042 ± 0.002 and 0.004 ± 0.003, respectively. The lower anisotropy for dimer relative to monomer apparently suggests a faster rotation of Trp in PEST dimer than monomer.

To extract more structural insights of PEST M1, its Trp fluorescence lifetime (τ) was determined. Figure 5b depicts the decay profile of Trp fluorescence intensity for PEST M1 dimer and its monomer. In both PEST monomer and dimer, two fluorescence lifetime of Trp was obtained from the decay analysis (Table 2). No significant change in Trp mean fluorescence lifetime was observed in PEST M1 dimer (2.83 ns) compared to monomer (2.88 ns). Trp fluorescence lifetime distribution profile of PEST M1 monomer and dimer also display insignificant changes (Figure 5c). The two lifetime species observed may arise from two unique conformations PEST fragment or existence of Trp rotamers that are quenched to different extents by nearby groups.

The fluorescence anisotropy decay of PEST M1 Trp was collected, to estimate its rotational correlation time (θ). Figure 5d displays the Trp anisotropy decay

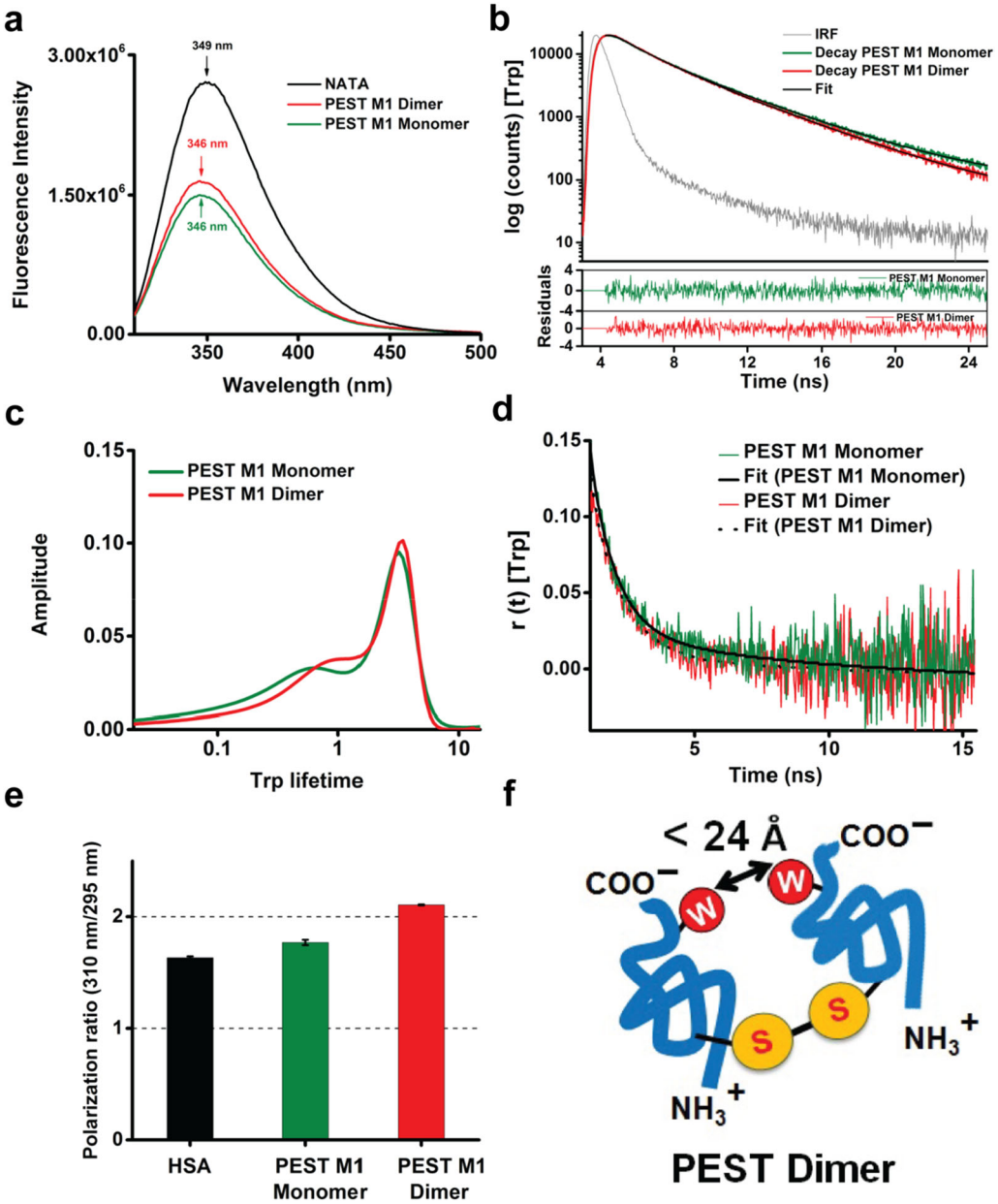

Figure 5. (**a**) Steady state fluorescence spectra; (**b**) fluorescence intensity decay profile (**c**) lifetime distribution and (**d**) Fitted anisotropy decay profile (λ_{ex} = 295 nm) of PEST M1 monomer [20 μM] and PEST M1 dimer [10 μM] at pH 7.4 in reducing and non-reducing condition, respectively. Residuals for fit are shown in bottom panel of intensity decay profiles. For MEM analysis, lifetime decay of each sample was fitted for 100 exponentials in the range of 0.01 ns to 15 ns of lifetime with 0.001 as initial value for flat distribution. (**e**) Shows polarization ratio of HSA, PEST M1 monomer and PEST M1 dimer at 310 and 295 nm. (**f**) Represents the proposed model for dimeric PEST fragment at pH 7.4.

of PEST M1 dimer and its monomer. PEST M1 dimer shows slightly faster anisotropy decay profile in comparison with PEST M1 monomer. Figure S5 (Supplementary Information) depicts the fitted anisotropy decay and its corresponding residuals for PEST M1 Trp in monomer and dimer. The anisotropy decay analysis of PEST M1 dimer and monomer shows two correlation times, a fast correlation time (θ_{fast}) of 1.0 and 0.94 ns with respective amplitude; 0.85 and 0.76, and a slow correlation time (θ_{slow}) of 6.6 and 6.8 ns with an amplitude of 0.15 and 0.24, respectively (Table 3). PEST M1 dimer reveals a higher fractional contribution of fast correlation time (θ_{fast}) to the decay relative to PEST M1 monomer. The relatively higher amplitude of fast correlation time (θ_{fast}) in PEST M1 is puzzling. Further, the global rotational correlation time for the dimer is also apparently faster than the monomer. This is unexpected, as the dimer with double the molecular weight of the monomer is expected to tumble slower than monomer.

Table 2. Average tryptophan fluorescence lifetime of PEST M1 dimer and monomer at pH 7.4. Values in brackets indicate standard deviations for n = 3.

PEST	$\chi^2_{reduced}$	τ_1(ns)	α_1	τ_2(ns)	α_2	Mean lifetime (ns)
Dimer	1.00	1.68 (0.09)	0.51	4.00 (0.06)	0.49	2.83 (0.05)
Monomer	1.01	1.61 (0.02)	0.49	4.13 (0.01)	0.51	2.88 (0.02)

Table 3. Tryptophan fluorescence anisotropy decay data of PEST M1 dimer and its monomer at pH 7.4. Values in brackets indicate standard deviations for n = 3.

PEST	χ^{2a}	r_0[b]	r_{ss}[c]	θ_1[d](ns)	β_1[e]	θ_2[d](ns)	β_2[e]
Dimer	1.00	0.13	0.047	1.00 (0.09)	0.85	6.6 (0.60)	0.15
Monomer	1.07	0.16	0.059	0.94 (0.02)	0.76	6.8 (0.20)	0.24

[a]Reduced χ^2 for the fit.

[b] apparent anisotropy from fit.

[c]Calculated anisotropy (steady state) from fit.

[d]Rotational correlation time(s);

[e]Fractional amplitude(s).

3.6 *Trp-Trp FRET Homotransfer in PEST M1 Dimer*

We have so far observed that both SEC (Figure 3a) and DLS data (Figure 3b) suggest a significantly larger Stokes radius for the dimer in comparison to the monomer (Table 1). Further, CD data (Figure 4 and Table 1) clearly point towards a more ordered structure for the PEST Wt and M1 dimer in comparison to their monomers. In this context, the slightly faster global rotational correlation time for the PEST M1 dimer (Figure 5d and Table 3) in comparison to the monomer appears counterintuitive.

Faster anisotropy decay can also occur in presence of Trp-Trp Förster Resonance Energy Homotransfer depending on the spatial proximity between the indole rings in the PEST M1 dimer. The Förster distance (R_0) for Trp-Trp homotransfer is reported to be 6-12 Å[26] We measured the polarization ratio of Trp at 310 and 295 nm excitation in both the PEST M1 monomer and dimer to determine if Trp-Trp homotransfer was occurring.[27] Figure 5e shows that while the control (HSA) and the PEST M1 monomer revealed a ratio below 2.0, PEST M1 dimer clearly showed a value above 2.0, indicating that homotransfer was indeed happening in the dimer.

As a consequence of homotransfer, the fluorescence anisotropy can decay rapidly *without* involving rotational diffusion. Indeed, analysis of the dimer decay (Table 3) reveals a faster than expected global rotational correlation time for the dimer and a higher amplitude for the fast correlation time ($\sim$1.0 ns). It is difficult to resolve the protein rotational dynamics component from the homotransfer component, making the dimer look deceptively dynamic as the monomer contrary to Stokes radii data.

FRET homotransfer implies the Trp in each chain cannot be farther than $2R_0$, about 24 Å from each other. Our earlier work has shown that the distance between Cys^9 and Trp^{70} in PEST monomer is about 31 Å[16] Consequently, the parallel orientation as proposed in Figure 5f appears as a possible structure for the PEST dimer. Presently it is not clear exactly how close the two chains are, but the marginal increase in β-strand content in the dimer, compared to monomer suggests the likelihood of inter-chain hydrogen bonding. Further, we see compaction or a minor collapse of the polypeptide chain upon dimer formation. This is evident from the Stokes radius of the dimer which is observed at $\sim$ 4 nm (Table 1) but would be expected near $\sim$ 4.7 nm for an expanded dimer. The chain collapse is probably driven by gain in amino acid side chain and backbone contacts, overcoming the conformational entropy[28] and favouring a structured disulphide bonded dimer. Indeed, the increased intra-residue contacts would drive the two chains of the

dimer closer, enhancing the homoFRET efficiency which is what we observe.

Disulphide bond formation in the eukaryotic cell is mediated by membrane-associated proteins Ero1 and Erv2 and soluble thiol-disulphide oxido-reductase, protein disulfide isomerase (PDI) in the endoplasmic reticulum.[29–31] Interestingly, PDI family of enzymes are reported to be actively involved in the proliferation, survival, and metastasis of several types of cancer cells. They are frequently upregulated in cancer cells compared to normal cells.[32] Presently it is not clear if PDI facilitates dimer formation of human c-Myc, improving its stability and leading to cancer.

Dimer formation has been shown to influence protein function. The short-lived tumour suppressor transcription factor p53, which contains a PEST region, binds to DNA in homodimeric form but not as monomer.[33] In vitro studies show, N-terminal region of MDM2 binds exclusively with C-terminal region of p53 dimer and targets p53 for proteasomal degradation, cytoplasmic localization and transcriptional repression.[34] Similarly, PEST containing c-Jun and c-Fos oncoproteins, act as transcription factors, forming c-Jun homodimer and Jun-Fos heterodimer. However, Jun-Fos heterodimer binds to DNA 25 times more efficient compared to c-Jun homodimer.[35] Intermolecular disulphide-bonded dimer in NEMO has been suggested to have a physiological role.[36] There are reports suggesting that c-Myc can have biological activity independent of Max like in control of endoreplication or RNA Polymerase III.[37] The possibility of Myc homo-oligomer regulating transcription in absence of Max in cells has been suggested.[38] Perhaps a more structured PEST region in the c-Myc homodimer may have a role in such a scenario. OmoMyc, a dominant-negative allele of Myc has been shown to form a stable disulphide-bonded homodimer that binds to DNA in the same way as MYC/MAX heterodimer.[39] Induction of OmoMyc has been shown to enable long-term suppression of tumour growth in mice[40,41] and believed to hold promise for treating human tumours.

In contrast to our observations here, no such significant structural change is induced upon dimer formation in Ribonucleotide reductase (RNR) regulatory protein Sml1.[4] However, it provides protection against proteolysis.[4] Perhaps an increase in the content of secondary structure in PEST fragment upon dimerization may confer protection against proteolysis and result in c-Myc stabilization *in vivo*. This needs further investigation.

4. Conclusions

In this work, the structural dynamics of intrinsically disordered human c-Myc PEST fragment was investigated upon formation of a disulphide-bonded dimer. CD results revealed that the dimer exhibited higher secondary structure content compared to the monomer. Further, the Trp moieties towards the C-terminus of the dimer displayed greater rotational mobility and marginally faster global rotational correlation times in comparison to the monomer, although the Stokes radii values were significantly higher for the dimer compared to monomer. This anomaly was traced to the transfer of excitation energy from one Trp to another in the dimer by the process of homoFRET, revealing their close spatial proximity. These results hint at a more ordered PEST dimer and perhaps close interactions between two polypeptide chains in the dimer. These results raise the possibility that c-Myc dimer formation may confer more stability compared to monomer, thereby prolonging its half-life in tumours.

Supplementary Information (SI)

Figure S1-S5 are available at https://www.ias.ac.in/chemsci.

Acknowledgements

RS is grateful to Department of Biotechnology (NER Division), New Delhi for funding support under project BT/409/NE/U-Excel/2013. The authors profusely appreciate the efforts of Dr. (Ms.) P. Lolla and Dr. (Ms.) R. Bhandari (CDFD, Hyderabad) for generating PEST constructs. They thank Prof. N. Periasamy (retired TIFR, Mumbai) for permitting the use of fluorescence intensity decay analysis software and Prof. G. Krishnamoorthy (retired TIFR, Mumbai) for discussions.

References

1. Wright P E and Dyson H J 2015 Intrinsically disordered proteins in cellular signalling and regulation *Nat. Rev. Mol. Cell. Biol.* **16** 18
2. Dunker A K, Brown C J, Lawson J D, Iakoucheva L M and Obradovic Z 2002 Intrinsic disorder and protein function *Biochemistry* **41** 6573
3. Dunker A K, Brown C J and Obradovic Z 2002 Identification and functions of usefully disordered proteins *Adv. Protein Chem.* **62** 25
4. Danielsson J, Liljedahl L, Barany-Wallje E, Sønderby P, Kristensen L H, Martinez-Yamout M A, Dyson H J, Wright P E, Poulsen F M and Mäler L 2008 The intrinsically disordered RNR inhibitor Sml1 is a dynamic dimer *Biochemistry* **47** 13428

5. Henriksson M and Luscher B 1996 *Advances in Cancer Research* (USA: Elsevier) p. 109
6. Marcu K B, Bossone S A and Patel A J 1992 Myc function and regulation *Annu. Rev. Biochem.* **61** 809
7. Spencer C A and Groudine M 1991 *Advances in cancer research* (USA: Elsevier) p.1
8. Treier M, Staszewski L M and Bohmann D 1994 Ubiquitin-dependent c-Jun degradation *in vivo* is mediated by the δ domain *Cell* **78** 787
9. Bies J and Wolff L 1997 Oncogenic activation of c-Myb by carboxyl-terminal truncation leads to decreased proteolysis by the ubiquitin-26S proteasome pathway *Oncogene* **14** 203
10. Andresen C, Helander S, Lemak A, Farès C, Csizmok V, Carlsson J, Penn L Z, Forman-Kay J D, Arrowsmith C H and Lundström P 2012 Transient structure and dynamics in the disordered c-Myc transactivation domain affect Bin1 binding *Nucleic Acids Res.* **40** 6353
11. Blackwell T K, Kretzner L, Blackwood E M, Eisenman R N and Weintraub H 1990 Sequence-specific DNA binding by the c-Myc protein *Science* **250** 1149
12. Prendergast G C and Ziff E B 1991 Methylation-sensitive sequence-specific DNA binding by the c-Myc basic region *Science* **251** 186
13. Rogers S, Wells R and Rechsteiner M 1986 Amino acid sequences common to rapidly degraded proteins: the PEST hypothesis *Science* **234** 364
14. Luscher B and Larsson L-G 1999 The basic region/helix–loop–helix/leucine zipper domain of Myc proto-oncoproteins: function and regulation *Oncogene* **18** 2955
15. Rechsteiner M and Rogers S W 1996 PEST sequences and regulation by proteolysis *Trends Biochem. Sci.* **21** 267
16. Ansari M Z and Swaminathan R 2020 Structure and Dynamics at N and C-terminal regions of Intrinsically Disordered Human c-Myc PEST Degron reveal a pH-induced transition *Proteins* **88** 889
17. Ansari M Z, Kumar A, Ahari D, Priyadarshi A, Lolla P, Bhandari R and Swaminathan R 2018 Protein charge transfer absorption spectra: an intrinsic probe to monitor structural and oligomeric transitions in proteins *Faraday Discuss.* **207** 91
18. Kumar S, Ravi V K and Swaminathan R 2008 How do surfactants and DTT affect the size, dynamics, activity and growth of soluble lysozyme aggregates? *Biochem. J.* **415** 275
19. Bevington P R and Robinson K D 1992 *Data reduction and error analysis for the physical sciences* 2nd edn. (McGraw-Hill, Inc.: New York)
20. Swaminathan R, Periasamy N, Udgaonkar J B and Krishnamoorthy G 1994 Molten globule-like conformation of barstar: a study by fluorescence dynamics *J. Phys. Chem.* **98** 9270
21. Livesey A K and Brochon J C 1987 Analyzing the distribution of decay constants in pulse-fluorimetry using the maximum entropy method *Biophys. J.* **52** 693
22. Skilling J and Bryan R K 1984 Maximum entropy image reconstruction-general algorithm *Mon. Not. R. Astron. Soc.* **211** 111
23. Homchaudhuri L, Kumar S and Swaminathan R 2006 Slow aggregation of lysozyme in alkaline pH monitored in real time employing the fluorescence anisotropy of covalently labelled dansyl probe *FEBS Lett.* **580** 2097
24. Tompa P 2002 Intrinsically unstructured proteins *Trends Biochem. Sci.* **27** 527
25. Csizmok V, Szollosi E, Friedrich P and Tompa P 2006 A novel two-dimensional electrophoresis technique for the identification of intrinsically unstructured proteins *Mol. Cell Proteom.* **5** 265
26. Van Der Meer B W, Coker G and Chen S Y S 1991 *Resonance energy transfer: theory and data* (Wiley-VCH: New York)
27. Moens P D J, Helms M K and Jameson D M 2004 Detection of tryptophan to tryptophan energy transfer in proteins *Protein J.* **23** 79
28. Dill K A and Bromberg S 2012 *Molecular driving forces: statistical thermodynamics in biology, chemistry, physics, and nanoscience* 2nd edn. (Garland Science: New York)
29. Goldberger R F, Epstein C J and Anfinsen C B 1963 Acceleration of reactivation of reduced bovine pancreatic ribonuclease by a microsomal system from rat liver *J. Biol. Chem.* **238** 628
30. Freedman R B 1984 Native disulphide bond formation in protein biosynthesis: evidence for the role of protein disulphide isomerase *Trends Biochem. Sci.* **9** 438
31. Sevier C S and Kaiser C A 2002 Formation and transfer of disulphide bonds in living cells *Nat. Rev. Mol. Cell. Biol.* **3** 836
32. Lee E and Lee D H 2017 Emerging roles of protein disulfide isomerase in cancer *BMB Rep.* **50** 401
33. Tarunina M and Jenkins J R 1993 Human p53 binds DNA as a protein homodimer but monomeric variants retain full transcription transactivation activity *Oncogene* **8** 3165
34. Katz C, Low-Calle A M, Choe J H, Laptenko O, Tong D, Joseph-Chowdhury J-S N, Garofalo F, Zhu Y, Friedler A and Prives C 2018 Wild-type and cancer-related p53 proteins are preferentially degraded by MDM2 as dimers rather than tetramers *Genes Dev.* **32** 430
35. Halazonetis T D, Georgopoulos K, Greenberg M E and Leder P 1988 c-Jun dimerizes with itself and with c-Fos, forming complexes of different DNA binding affinities *Cell* **55** 917
36. Herscovitch M, Comb W, Ennis T, Coleman K, Yong S, Armstead B, et al. 2008 Intermolecular disulfide bond formation in the NEMO dimer requires Cys54 and Cys347 *Biochem. Biophys. Res. Commun.* **367** 103
37. Steiger D, Furrer M, Schwinkendorf D and Gallant P 2008 Max-independent functions of Myc in Drosophila melanogaster *Nat. Genet.* **40** 1084
38. Dang C V 2012 MYC on the path to cancer *Cell* **149** 22
39. Jung L A, Gebhardt A, Koelmel W, Ade C P, Walz S, Kuper J, et al. 2017 OmoMYC blunts promoter invasion by oncogenic MYC to inhibit gene expression characteristic of MYC-dependent tumors *Oncogene* **36** 1911
40. Soucek L, Whitfield J, Martins C P, Finch A J, Murphy D J, Sodir N M, et al. 2008 Modelling Myc inhibition as a cancer therapy *Nature* **455** 679
41. Annibali D, Whitfield J R, Favuzzi E, Jauset T, Serrano E, Cuartas I, et al. 2014 Myc inhibition is effective against glioma and reveals a role for Myc in proficient mitosis *Nat. Commun.* **5** 1